Two-dimensional simple proportional feedback control of a chaotic reaction system

Ankur Mukherjee,[1] Dominic P. Searson,[1] Mark J. Willis,[1,*] and Stephen K. Scott[2]
[1]*School of Chemical Engineering and Advanced Materials, Newcastle University, Newcastle upon Tyne, NE1 7RU, United Kingdom*
[2]*School of Chemistry, Faculty of Mathematics and Physical Sciences, University of Leeds, Leeds, LS2 9JT, United Kingdom*
(Received 28 September 2007; revised manuscript received 21 January 2008; published 21 April 2008)

The simple proportional feedback (SPF) control algorithm may, in principle, be used to attain periodic oscillations in dynamic systems exhibiting low-dimensional chaos. However, if implemented within a discrete control framework with sampling frequency limitations, controller performance may deteriorate. This phenomenon is illustrated using simulations of a chaotic autocatalytic reaction system. A two-dimensional (2D) SPF controller that explicitly takes into account some of the problems caused by limited sampling rates is then derived by introducing suitable modifications to the original SPF method. Using simulations, the performance of the 2D-SPF controller is compared to that of a conventional SPF control law when implemented as a sampled data controller. Two versions of the 2D-SPF controller are described: linear (L2D-SPF) and quadratic (Q2D-SPF). The performance of both the L2D-SPF and Q2D-SPF controllers is shown to be superior to the SPF when controller sampling frequencies are decreased. Furthermore, it is demonstrated that the Q2D-SPF controller provides better fixed point stabilization compared to both the L2D-SPF and the conventional SPF when concentration measurements are corrupted by noise.

DOI: 10.1103/PhysRevE.77.046215 PACS number(s): 05.45.−a, 82.40.Bj

I. INTRODUCTION

The control of chaos in nonlinear dynamic systems by stabilizing an existing unstable periodic orbit (UPO) by the Ott-Greborgi-Yorke (OGY) method is well known [1]. Analysis and exploitation of chaotic behavior to achieve system performance improvements have since received widespread attention [2–8]. Along with the OGY algorithm, numerous other strategies have been proposed in the literature for the control of chaos [5,6]. The simple proportional feedback (SPF) control law proposed by Peng *et al.* [3] is a geometrically inspired variant of the OGY technique and has proved to be popular for controlling chaos in chemical and biological systems. For instance, the SPF law has been used to control chaos in an isothermal three-variable autocatalator model [3] in combustion reactions of CO and H_2 [9] and modifications of it have been used to control chaotic oscillations in a copper-phosphoric acid system under potentiostatic conditions [10] and to stabilize cardiac arrhythmias [11].

This paper addresses the issue of implementation of the SPF algorithm in a discrete sampled data control framework. The objective of this paper is to compare, using simulations of a chaotic reaction system, the performance of the SPF algorithm [3] with a proposed generalization of the SPF control law. The generalization of the SPF algorithm is intended to provide superior control when implemented in a discrete control framework with the measured variable having sampling frequency limitations.

The effect of the sampling frequency on the performance of the conventional SPF controller in a discrete framework system is investigated. It is shown using simulations that as the sampling frequency is decreased the performance of the SPF controller may deteriorate. Hence, the choice of the sampling frequency of the SPF controller in a discrete control system is critically important for its successful implementation.

To improve control performance when sampling limitations degrade the performance of SPF, two modifications of SPF are proposed: linear discrete (L2D-SPF) and quadratic discrete (Q2D-SPF). Both algorithms are shown to provide superior control of the chaotic reaction system with sampling limitations.

The paper is organized as follows. In Sec. II the SPF algorithm for the control of low-dimensional chaotic systems is briefly discussed as well as some existing SPF modifications from the literature. We also discuss some problems that can arise when implementing SPF within a sampled data framework. In Sec. III the model of the mutating autocatalytic chemical reaction system is presented and the standard SPF controller is used to control a product concentration. It is then demonstrated that a reduction in controller sampling frequency causes deterioration in controller performance. Our extensions to SPF are derived in Sec. IV. When applied to the simulated reaction system these algorithms are shown to provide improved control of product concentration. The paper concludes with a discussion in Sec. V.

II. SIMPLE PROPORTIONAL FEEDBACK

A. Dynamic system description

A continuous autonomous dynamic system may be described by p coupled ordinary differential equations, where p represents the number of state variables comprising the system and $\mathbf{x}\in\mathbf{R}^p$ is the state vector at time t where $t\geq 0$. The time derivative of the system state at time t is denoted by $\dot{\mathbf{x}}\in\mathbf{R}^p$:

$$\dot{\mathbf{x}} = f(\mathbf{x},u), \tag{1}$$

*Corresponding author. FAX: +44 (0)191 222 5292. mark.willis@newcastle.ac.uk

$$\mathbf{y} = h(\mathbf{x}). \tag{2}$$

The function f: $\mathbf{R}^p \times \mathbf{R}^1 \rightarrow \mathbf{R}^p$ is a smooth nonlinear vector function of $\mathbf{x}$ and u. In addition, $\mathbf{y} \in \mathbf{R}^q$ is the system output and measurement vector at time t. The q system outputs are defined by the measurement function h: $\mathbf{R}^p \rightarrow \mathbf{R}^q$, which is a smooth nonlinear vector function of $\mathbf{x}$. For simplicity, in this work it is assumed that all states of the system are directly observable, hence $p=q$ and $\mathbf{y}=\mathbf{x}$. The scalar u is the manipulated variable (this can be an external forcing variable or a changeable system parameter) at time t. The initial condition for the system is defined as $\mathbf{x}_0$, and it is assumed that the system exhibits chaotic behavior for the chosen $\mathbf{x}_0$ when u is close to its nominal value $\bar{u}$.

B. SPF control law

The SPF algorithm employs the use of a Poincaré section which, for a p-dimensional system, is a $(p-1)$-dimensional hyperplane in the state space that intersects the trajectory of the dynamic system of interest [5]. The Poincaré section may be used to form a discrete mapping, known as the Poincaré map, of the values of a measured output y at successive intersections $-y_n$, y_{n+1}, etc., of the chaotic trajectory with the section. The Poincaré map F for the dynamic system with nominal manipulated variable $\bar{u}$ may be represented by Eq. (3). The value of y_n for which $y_{n+1}=y_n$ is the fixed point of this map, $y_f(\bar{u})$:

$$y_{n+1}(\bar{u}) = F(y_n, \bar{u}). \tag{3}$$

The SPF algorithm directly stabilizes the fixed point of the Poincaré map by applying a small perturbation δu_n to $\bar{u}$ to generate the control signal u_n. The perturbation is proportional to the error Δy between the fixed point and the measured variable y_n at the current intersection of the trajectory with the Poincaré section [18]:

$$\delta u_n = \frac{m_1 \Delta y}{(m_1 - 1)\dfrac{dy_f(\bar{u})}{du}} = \frac{1}{g}\Delta y, \tag{4}$$

where the constant g is defined as

$$g \equiv \frac{(m_1 - 1)}{m_1}\frac{dy_f(\bar{u})}{du} \tag{5}$$

and m_1 is the gradient of the Poincaré map at $y_f(\bar{u})$. The quantity $\frac{dy_f(\bar{u})}{du}$ is the observed change in the position of the fixed point when a small test perturbation δu is made to the manipulated variable. It can be seen that Eq. (4) represents a proportional feedback scheme where the size of the control action is directly proportional to the deviation of the current value of y at the Poincaré section y_n from the desired fixed point $y_f(\bar{u})$. Note that the control action computed by Eq. (4) is only used when the intersection of the system trajectory with the Poincaré section is "close" to the fixed point—i.e., when $\Delta y \leq \varepsilon$ where ε is a small user-defined threshold. If $\Delta y > \varepsilon$, then $\delta u_n = 0$.

C. Modifications to SPF

The application of a small perturbation has the secondary effect of displacing the fixed point of F and a theoretical limitation of the SPF algorithm is that it requires this displacement of the fixed point to be along the attractor. It was shown by Petrov *et al.* [12] that in some instances when this condition is violated, the SPF algorithm is unable to successfully generate closed loop control, even though the Poincaré map is one dimensional in nature. Petrov *et al.* [12] further suggested using a linear combination of manipulated variables to mitigate such shifts in position of the fixed point of the Poincaré map. This method was further developed by a recursive proportional feedback algorithm, proposed by Rollins *et al.* [13]. The recursive term counteracts the changes in position of the fixed point by including a component of the previous manipulated variable perturbation δu_{n-1} into the current manipulated variable value u_n. The recursive algorithm mitigates errors caused by changes in the position of the Poincaré map when the fixed point is not along the attractor. However, the shifts in the Poincaré map considered in [17] are not due to sampling restrictions which we address in this paper by developing an extension of the SPF algorithm for application in a discrete control framework to counteract effects of limited frequency state variable measurements. The movements in the Poincaré map in this case are perpendicular to the Poincaré section and along the attractor. The resultant Poincaré map is defined to be a function of the position of the Poincaré section in the phase space. We assume that any changes in position of the fixed point are along the attractor and previous manipulated variable perturbations δu_{n-1} are not used to influence the current manipulated variable u_n.

D. Limitations of SPF within a discrete control framework

An important feature in sampled data control systems is the choice of sampling intervals. With electronic controllers this choice is simple: sample as fast as possible. However, sampling too fast with digital control systems is not always desirable because, for instance, the implementation costs will increase because more capable components must be installed. Furthermore, high-frequency components—such as noise—will also be captured in the signal. This is not necessarily beneficial to the performance of the control loop. Conversely, if the sampling rate is too slow, then signal loss will occur. Hence, the choice of an appropriate sampling interval should be based on the dynamics of the process being controlled. The primary requirement is that the sampling operation must return the key dynamic characteristics of the process.

The SPF controller directly stabilizes the unstable fixed point of the map and, in idealized conditions (in a noise free continuous control system), one single manipulated variable perturbation stabilizes the trajectory to periodic oscillations. In practice, however, this is not the case. This is because there are a number of assumptions and approximations inherent in the derivation of the SPF control law that are violated to some degree. For example, the next return map will actually be slightly nonlinear around the fixed point and—

importantly—intersections of the system trajectory with the infinitesimally thin Poincaré section cannot necessarily be detected in a discrete controller framework. The accuracy of detection of these intersections is a critically important requirement for successful implementation of the SPF controller in data sampled control systems. This accuracy in turn depends on the sampling interval employed. Hence, in simulations and experimental implementations, pragmatic modifications to the procedure are made. If the Poincaré section cannot be located accurately due to sampling restrictions, then interpolations or functional approximations to the next return map are used. Or because it is not possible to detect intersections with an infinitely thin plane, practical realizations of the SPF controller must use intersections of the system trajectory with a user-defined Poincaré "region" of sufficient finite thickness. In the remainder of this paper it will be shown—using a case study simulation of an autocatalytic reaction system—how the effects of decreasing sampling frequency with a finite thickness Poincaré "region" can cause deterioration in the performance of the discrete SPF controller. It will also be shown how the SPF algorithm may be modified to compensate for these effects. In the next section, the dynamic system used for the case study is briefly described followed by how it may be controlled, using the standard SPF algorithm, when the finite Poincaré region is very thin and the controller sampling frequency is fast.

III. SPF CONTROL OF AN AUTOCATALYTIC CHEMICAL REACTION MODEL

Chaos is found in many chemical processes because of the inherently nonlinear nature of chemical systems and often structurally unstable dynamics. The presence of nonlinear feedback mechanisms in autocatalytic reaction systems is responsible for a multiplicity of steady states, oscillations, and potential chaotic behavior [14]. Gray and Scott introduced a model based on cubic autocatalysis [15–17] which showed chaotic oscillations in certain parameter regions. Here, the mutating autocatalator model proposed by Abasaeed [14] is used. In this model, the autocatalyst mutates to another form and competes with the original autocatalyst for its subsequent regeneration.

A. Autocatalytic system model

The overall reaction converts reactant A (autocatalyzed by B and C) to products P_1 and P_2 within an isothermal continuous stirred tank reactor (CSTR). The model consists of five reaction steps in which the autocatalytic species B and C compete for reactant A, but produce different products P_1 and P_2.

In order to reduce the number of independent variables in the model, and hence facilitate subsequent analysis, the differential equations representing the system may be transformed into semidimensionless forms as shown by Eqs. (6)–(10) where X is the dimensionless extent of reactant A consumption and Y and Z are the dimensionless reaction extents of B and C concentrations, respectively. Y_f and Z_f are the dimensionless feed concentrations of B and C into the CSTR. In addition, θ is the residence time of the CSTR, γ_1 and γ_2 are model constants related to the constant feed concentration of A and the underlying kinetic rate constants, and α and β are constants dictating the relative strength of the autocatalytic growth of the two species and relative rate of the reactions. The dimensionless concentrations of the products P_1 and P_2 are represented by $\bar{P}_1$ and $\bar{P}_2$, respectively:

$$\text{reactant } A: \quad \dot{X} = -\frac{X}{\theta} + (1+\alpha)\gamma_1(1-X)Y^2 + \beta\gamma_1(1-X)Z^2, \tag{6}$$

$$\text{autocatalyst } B: \quad \dot{Y} = \frac{Y_f - Y}{\theta} + (1-\alpha)\gamma_1(1-X)Y^2 - \gamma_2 Y, \tag{7}$$

$$\text{autocatalyst } C: \quad \dot{Z} = \frac{Z_f - Z}{\theta} + \beta\gamma_1(1-X)Z^2 + 2\alpha\gamma_1(1-X)Y^2 - \frac{\gamma_2}{\beta}Z, \tag{8}$$

$$\text{product } P_1: \quad \dot{\bar{P}}_1 = \gamma_2 Y - \frac{\bar{P}_1}{\theta}, \tag{9}$$

$$\text{product } P_2: \quad \dot{\bar{P}}_2 = Z\frac{\gamma_2}{\beta} - \frac{\bar{P}_2}{\theta}. \tag{10}$$

The phase space for the system is three dimensional; i.e., it is not necessary to specify the values of the dimensionless product concentrations $\bar{P}_1$ and $\bar{P}_2$ to uniquely determine the state of the system.

B. Model parameters

The effect of the mutation coefficient α and the mutation efficiency β on the dynamic behavior of the system and selectivity performances were reported by Abasaeed [14] and Davies and Scott [18]. In their studies, the residence time θ was used as the adjustable system parameter for different combinations of α and β. Chaotic oscillations were observed with the following model parameters [14,18]: $\gamma_1=450$, $\gamma_2=11.25$, $Y_f=0.0667$, $Z_f=0$, $\alpha=0.29$, and $\beta=0.28$. Hence, these model parameter values were used for the simulations in this paper. In this model, species A and B are present in the CSTR feed stream, but C is not. The initial values of X, Y, and Z in the CSTR for the simulations were specified as $X_0=0.428$, $Y_0=0.328$, and $Z_0=0.1154$ [19].

C. Implementation of SPF on the autocatalytic system under near-ideal conditions

In this section the closed loop behavior of the autocatalytic reaction system under SPF control in near ideal conditions—i.e., with a very thin Poincaré region, a high sampling frequency, and no measurement noise—is examined. Following Davies and Scott [18], the theoretical

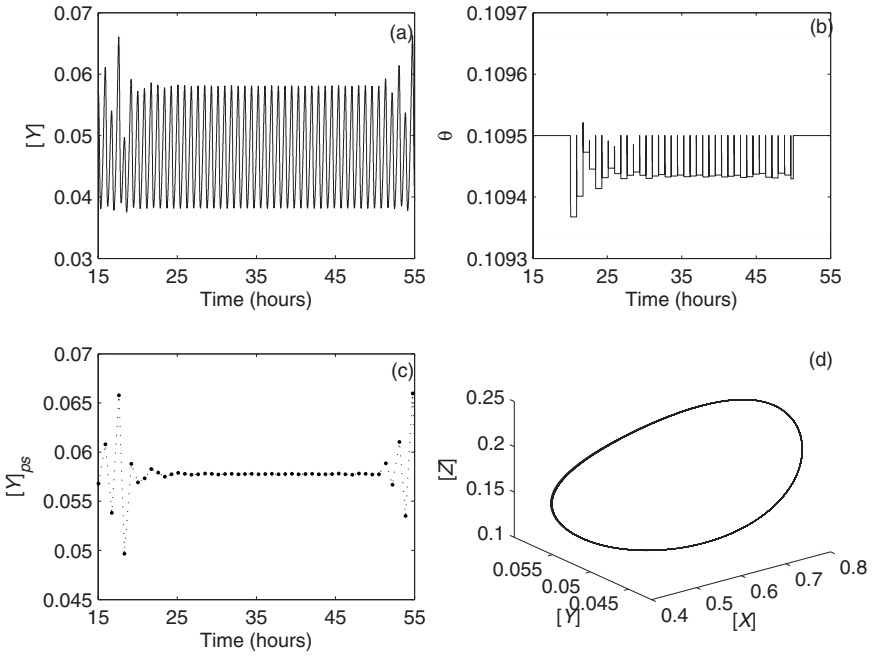

FIG. 1. Results for SPF control law for stabilization of an UPO under pseudocontinuous conditions (no noise). Panel (a): time series of dimensionless Y concentrations in the presence and absence of control action. Panel (b): instantaneous manipulated variable values.Panel (c): Y concentrations in the thin Poincaré region. Panel (d): phase portraits of time series of X, Y, and Z during closed-loop control.

Poincaré section selected as the basis for the study is formed by the plane at $X=0.50$. When constructing the next return map, only the section transecting the upper part of the attractor is used. This is achieved by mapping only intersections of the trajectory with the Poincaré section from one direction—i.e., when the value of Z is changing such that $\frac{dZ}{dt}>0$. A Poincaré map for the nominal value of $\theta=0.1095$ and for a test perturbation ($d\theta=10^{-4}$) in θ was constructed. The change in θ was achieved by adjusting the flow rate into the simulated CSTR. The numerical integration step time for all the simulations in this paper is 10^{-3} h.

High-frequency (sample time $T_s=10^{-3}$ h) measurements of the reactant and product concentrations were made available—i.e., at a rate so fast that the SPF algorithm can essentially be considered as one that emulates continuous control. A Poincaré region was specified as $0.49\leq X\leq 0.51$. This "thin" Poincaré region—as far as is practically possible, i.e., within the limits of the integration time step for the differential equation model—closely approximates the theoretical Poincaré section in the phase space and ensures that all intersections of the "plane" are detected.

Davies and Scott [18] implemented the SPF method on the dimensionless model and studied the variation in product selectivity for a number of stabilized periodic orbits. Their work demonstrated that chaotic behavior is exhibited by this model over a range of residence time values above the lower Hopf bifurcation point $\theta=0.1089$. It was reported that the range of chaotic behavior was 1.675×10^{-3} residence time units (hours) wide. The measured output variable y was Y, the dimensionless concentration of species B in the CSTR. The manipulated variable was specified as the instantaneous residence time θ of the CSTR.

Following Davies and Scott [18], the SPF controller was used to regulate the dimensionless concentration of B in the CSTR and hence eliminate chaotic oscillations. The control action was switched on at time $t=20$ h (by which time the system trajectory had entered the chaotic attractor) and was switched off at time $t=50$ h after which the system was left in open loop for 10 h.

After the SPF controller is switched on at $t=20$ h, the system remains in open loop for 146.70 s until there is an intersection of the system trajectory with the Poincaré region close to the fixed point of the Poincaré map. The first manipulated variable update then occurs and closed-loop control is initiated. After the controller is switched off at $t=50$ h, the trajectory reverts to chaotic behavior. Figure 1(a) shows the time series plot of the Y concentrations in both the presence and absence of the control action, and Fig. 1(b) shows the manipulated variable values during the experiment. The values of Y at the thin Poincaré region are shown in Fig. 1(c). Finally, Fig. 1(d) depicts the phase portraits of the time series of the X, Y, and Z variables during closed-loop control. Note that the straight line plot of Y values (when the trajectory first enters the thin Poincaré region during each loop in the phase space) in Fig. 1(c) signifies that limit cycle behavior has been obtained by the SPF control algorithm; i.e., the trajectory intersects the thin Poincaré region at virtually the same point for each orbit around the attractor.

D. Effect of sampling frequency on controller performance

With the SPF control law, it may be expected that by increasing the controller sampling time interval, the control performance will be affected because it will be more difficult to determine the precise instant when the system trajectory intersects the Poincaré region. A thin Poincaré region, i.e., which may be defined as $0.49\leq X\leq 0.51$, the "mimic" of the theoretical Poincaré section, is used in the simulations here. The performance of the SPF controller under different sampling frequencies may be compared by identifying how closely it approaches the desired fixed point on every intersection of the trajectory (every loop in the phase space in closed loop conditions) with the Poincaré section. This prop-

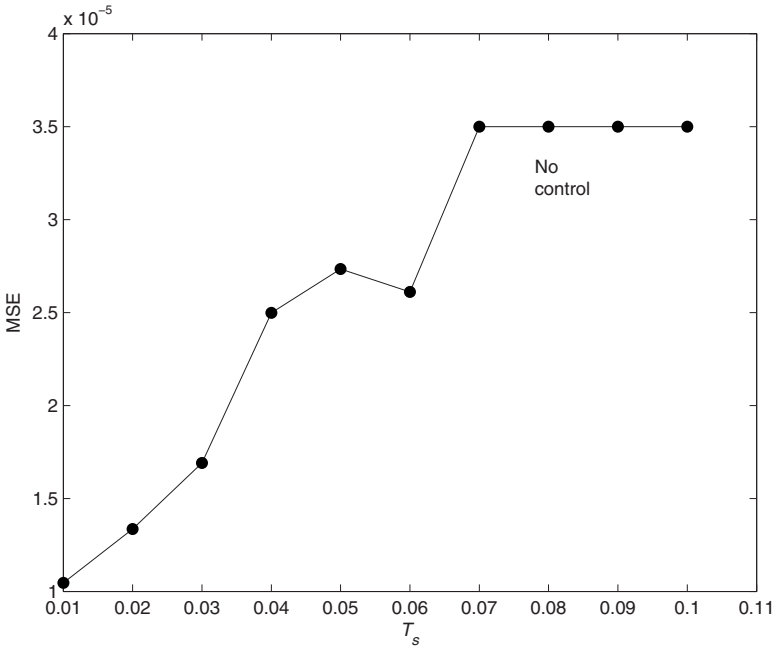

FIG. 2. Comparison of SPF controller performances in terms of the MSE of a period-1 fixed-point target with increasing sample time interval T_s (hours). Poincaré region defined as $0.49 \leq X \leq 0.51$.

erty is quantified by calculating the mean squared error σ_{MSE} of the intersected point of the trajectory on the Poincaré section with the actual fixed point of the Poincaré map. The theoretical point of intersection of the trajectory with the Poincaré section is located by following the trajectory at every integration time step of the ODE model. Mathematically, it may be expressed as

$$\sigma_{\mathrm{MSE}} = \frac{\sum_{j=1}^{M} (y_j^{sim} - y_f)^2}{M}, \tag{11}$$

where y_j^{sim} is the intersected point of the simulated trajectory with the Poincaré section, y_f is the fixed point of the Poincaré map, and M is the total number of intersections of the trajectory with the Poincaré section during closed-loop control.

A plot of the MSE values for the SPF controller when the sample time interval is progressively increased is shown in Fig. 2. From the figure, it may be seen that the MSE increases progressively as the sample time interval is increased. When the sample time interval increases beyond $T_s = 0.07$ h, no period-1 control is achieved by the SPF algorithm. Hence, when the sampling frequency is low due to restrictions on online process measurement capabilities, it is necessary to define a wider Poincaré region to ensure that the algorithm can successfully detect when the sampled trajectory is close to the theoretical Poincaré section. However, even with a wider Poincaré region, successful or tight closed-loop control by use of the traditional SPF algorithm may not be possible. The SPF control performance may degrade as the measurement sampling frequency is decreased even though the SPF controller applies manipulated variable perturbations while the system trajectory is within the Poincaré region. This is because the manipulated variable perturbation is computed to be proportional to the error $y - y_f$. However, the y_f used in the control law corresponds to the fixed point of the theoretical Poincaré section ($X = 0.50$ or very near to it), instead of using the fixed point of the Poincaré map at the current sampled point in the Poincaré region. As a result, the SPF algorithm does not target the correct fixed point. This causes progressive deterioration in control performance when the sampling frequency is decreased. The nonlinear dependence of the true fixed point on the sampled position in the Poincaré region causes deterioration in the controller performance.

IV. TWO-DIMENSIONAL SPF CONTROL

To improve controller performance, two control laws are proposed which explicitly formulate the Poincaré map as being X location dependent—i.e., a surface as shown in Fig. 3. A linear two-dimensional controller (L2D-SPF) and a quadratic two-dimensional controller (Q2D-SPF) are developed. The L2D-SPF control law assumes that the fixed point of the Poincaré map varies linearly within the Poincaré region of the phase space, while the Q2D-SPF assumes a quadratic relationship between the fixed point and the X location.

A. Derivation of the L2D-SPF and Q2D-SPF control laws

A Poincaré surface G is defined by the following relation, which may be thought of as specifying a different Poincaré map for each combination of values taken by u and X:

$$y_{n+1}(u,X) = G(y_n,u,X). \tag{12}$$

This may be linearized in the vicinity of the fixed point $y_f(\bar{u},\bar{X})$ of the map corresponding to the nominal manipulated variable $\bar{u}$ at the nominal location $\bar{X}$ of the infinitely thin Poincaré section:

$$y_{n+1}(\bar{u},\bar{X}) = m_1[y_n(\bar{u},\bar{X}) - y_f(\bar{u},\bar{X})] + m_2[y_f(\bar{u},\bar{X} + \delta X) - y_f(\bar{u},\bar{X})] + y_f(\bar{u},\bar{X}), \tag{13}$$

where m_1 is the gradient of the nominal Poincaré map at

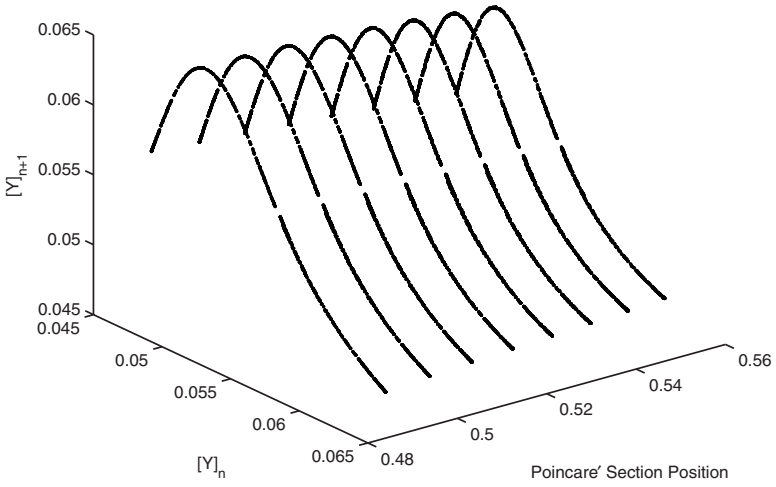

FIG. 3. A Poincaré surface in three-dimensional phase space of the autocatalytic reaction system. The Poincaré surface comprises individual Poincaré maps and is X location dependent.

$y_f(\bar{u},\bar{X})$ and m_2 is the gradient of the fixed points $y_f(\bar{u},\bar{X}+\delta X)$ in a direction orthogonal to the theoretical Poincaré section.

When the manipulated variable is perturbed by a small quantity δu, then the position of the fixed point is also perturbed. If it is assumed that the small perturbation does not significantly change the gradients m_1 and m_2, then

$$y_{n+1}(\bar{u}+\delta u,\bar{X}) = m_1[y_n(\bar{u},\bar{X}) - y_f(\bar{u}+\delta u,\bar{X})] + m_2[y_f(\bar{u}+\delta u,\bar{X}+\delta X) - y_f(\bar{u}+\delta u,\bar{X})] + y_f(\bar{u}+\delta u,\bar{X}). \tag{14}$$

Again, the fixed point of the perturbed system—for some small δu—may be written as a first-order Taylor series expansion around the fixed point of the nominal system,

$$y_f(\bar{u}+\delta u,\bar{X}) = y_f(\bar{u},\bar{X}) + \delta u\frac{\partial y_f(\bar{u},\bar{X})}{\partial u}, \tag{15}$$

and also for the perturbed system at a displacement δX from the location of the infinitely thin Poincaré section,

$$y_f(\bar{u}+\delta u,\bar{X}+\delta X) = y_f(\bar{u},\bar{X}+\delta X) + \delta u\frac{\partial y_f(\bar{u},\bar{X}+\delta\bar{X})}{\partial u}. \tag{16}$$

For $u=\bar{u}$, any intersection with the nominal Poincaré section located at $\bar{X}$ can be written as

$$y_n(\bar{u},\bar{X}) = y_f(\bar{u},\bar{X}) + \Delta y. \tag{17}$$

Substitution of Eqs. (15)–(17) into (14) gives

$$y_{n+1}(\bar{u}+\delta u,\bar{X}) = m_1\left(y_f(\bar{u},\bar{X}) + \Delta y - y_f(\bar{u},\bar{X}) - \delta u\frac{\partial y_f(\bar{u},\bar{X})}{\partial u}\right) + m_2\left(y_f(\bar{u},\bar{X}+\delta X) + \delta u\frac{\partial y_f(\bar{u},\bar{X}+\delta X)}{\partial u} - y_f(\bar{u},\bar{X}) - \delta u\frac{\partial y_f(\bar{u},\bar{X})}{\partial u}\right) + y_f(\bar{u},\bar{X}) + \delta u\frac{\partial y_f(\bar{u},\bar{X})}{\partial u}. \tag{18}$$

To ensure closed loop regulation δu must be specified such that

$$y_{n+1}(\bar{u}+\delta u,\bar{X}) = y_f(\bar{u},\bar{X}). \tag{19}$$

Therefore Eq. (12) becomes

$$0 = m_1\left(\Delta y - \delta u\frac{\partial y_f(\bar{u},\bar{X})}{\partial u}\right) + m_2\left(y_f(\bar{u},\bar{X}+\delta X) - y_f(\bar{u},\bar{X}) + \delta u\frac{\partial y_f(\bar{u},\bar{X}+\delta X)}{\partial u} - \delta u\frac{\partial y_f(\bar{u},\bar{X})}{\partial u}\right) + \delta u\frac{\partial y_f(\bar{u},\bar{X})}{\partial u}. \tag{20}$$

Assuming that $\frac{\partial y_f(\bar{u},\bar{X})}{\partial u} = \frac{\partial y_f(\bar{u},\bar{X}+\delta X)}{\partial u}$ and defining $\Delta x = y_f(\bar{u},X+\delta X) - y_f(\bar{u},\bar{X})$ gives

$$(m_1-1)\,\delta u\frac{\partial y_f(\bar{u},\bar{X})}{\partial u} = m_1\Delta y + m_2\Delta x. \tag{21}$$

This yields the control law

$$\delta u = \frac{m_1\Delta y + m_2\Delta x}{(m_1-1)\dfrac{\partial y_f(\bar{u},\bar{X})}{\partial u}} = \frac{1}{g}\Delta y, \tag{22}$$

where

$$g \equiv \frac{(m_1-1)}{m_1 + m_2\left(\dfrac{\Delta x}{\Delta y}\right)}\frac{\partial y_f(\bar{u},\bar{X})}{\partial u}. \tag{23}$$

Equation (22) represents a SPF control law where the magnitude of the control action is proportional to the deviation Δy from the desired fixed point. Note also that the parameter g is dependent on Δy and Δx and is not constant as with the conventional SPF algorithm.

A similar control law may be derived assuming that the fixed point of the Poincaré map has a quadratic dependence

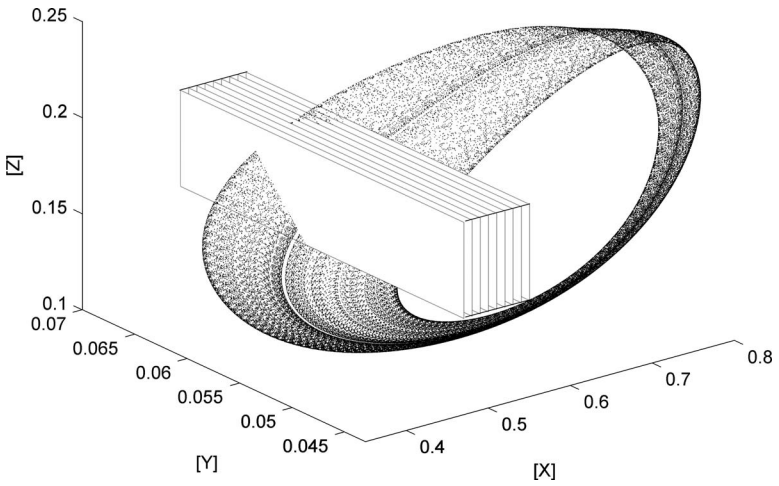

FIG. 4. A "wide" three-dimensional Poincaré region defined as $0.44 \leq X \leq 0.56$.

on the distance in the X dimension of the Poincaré region:

$$y_{n+1}(\bar{u},\bar{X}) = m_1[y_n(\bar{u},\bar{X}) - y_f(\bar{u},\bar{X})] + m_2[y_f(\bar{u},\bar{X}+\delta X) - y_f(\bar{u},\bar{X})] + m_3[y_f(\bar{u},\bar{X}+\delta X) - y_f(\bar{u},\bar{X})]^2 + y_f(\bar{u},\bar{X}). \quad (24)$$

Following the previous derivation yields the control law

$$\delta u = \frac{m_1\Delta y + m_2\Delta x + m_3\Delta x^2}{(m_1-1)\dfrac{\partial y_f(\bar{u},\bar{X})}{\partial u}} \equiv \frac{1}{g}\Delta y, \quad (25)$$

where the control constant g is in this case defined by

$$g \equiv \frac{(m_1-1)}{m_1 + m_2\left(\dfrac{\Delta x}{\Delta y}\right) + m_3\left(\dfrac{\Delta x^2}{\Delta y}\right)} \frac{\partial y_f(\bar{u},\bar{X})}{\partial u}. \quad (26)$$

B. Estimation of controller coefficients

The m_1 coefficient is the slope of the nominal Poincaré map at its fixed point. In order to implement the L2D-SPF and Q2D-SPF control algorithms, the additional coefficients m_2 and m_3 may be calculated by generating a linear (or polynomial) fit of the dependence of the fixed point on the sampled point in the Poincaré region of the phase space. To calculate this dependence for the autocatalator model, ten different Poincaré maps were constructed within the region $0.44 \leq X \leq 0.56$. The locations of the corresponding thin Poincaré "subregions" were specified such that they were equally spaced across this interval as indicated in Fig. 4. Given sufficient concentration data, a series of Poincaré maps may be constructed: one for each subregion. A positive perturbation in the residence time equaling $\delta\theta = 10^{-4}$ was used to generate a perturbed Poincaré map for each subregion, and each fixed point was calculated from the corresponding next return maps (i.e., by locating the intersection of the next return map with the bisectrix). After calculating the fixed points, linear and quadratic relationships between the nominal fixed point and the subregions' fixed points were obtained using least-squares regression. The dependence of the fixed point on the position of the center of each subregion is shown in Fig. 5. For the linear fit the coefficient of determination $R^2 = 0.78$, and for the quadratic fit $R^2 = 0.99$.

Once the controller coefficients have been computed, Eqs. (23) and (26) may be used to calculated the controller gains g at a given Δy and Δx for the L2D-SPF and Q2D-SPF controllers, respectively. For the autocatalator model, Figs. 6 and 7 show the dependence of the controller gain for different values of Δy and Δx. The distance of the fixed point from the nominal fixed point is plotted on the abscissa whereas the corresponding controller gain is shown on the ordinate for a certain deviation Δy from the nominal fixed point. Controller gains for four different Δy deviations (uniformly spaced between -0.002 and 0.002) are shown. The controller gain at $\Delta x = 0.0$ represents the gain at the fixed point of the nominal Poincaré section at $X = 0.50$.

C. Comparative performance of L2D-SPF and Q2D-SPF control laws

To compare the performance of the two algorithms, the sampling time T_s was set to 10^{-2} h. In the implementation of both control algorithms, the control action was switched on at time $t = 20$ h and was switched off at time $t = 50$ h. The system was then left to run in open loop for a further 10 h. The relative performance of each algorithm was only assessed using data from the period 20–50 h.

Figure 8 shows the comparative performances of the L2D-SPF and Q2D-SPF controllers. Figures 8(a) and 8(c) show the time series plot of the Y concentrations using the L2D-SPF and the Q2D-SPF controllers, respectively. Figures 8(b) and 8(d) show the Y concentrations within the nominal thin Poincaré region at $X = 0.5$. Note that while both controllers successfully stabilize the fixed point, the Q2D-SPF controller provides superior control performance.

The performances of the respective controllers were also evaluated when noise was added to the concentration measurements. Gaussian noise was added independently to the time series measurements of X, Y, and Z. In each case the standard deviation of the noise was set to 0.50% of the standard deviation of the corresponding signal obtained during

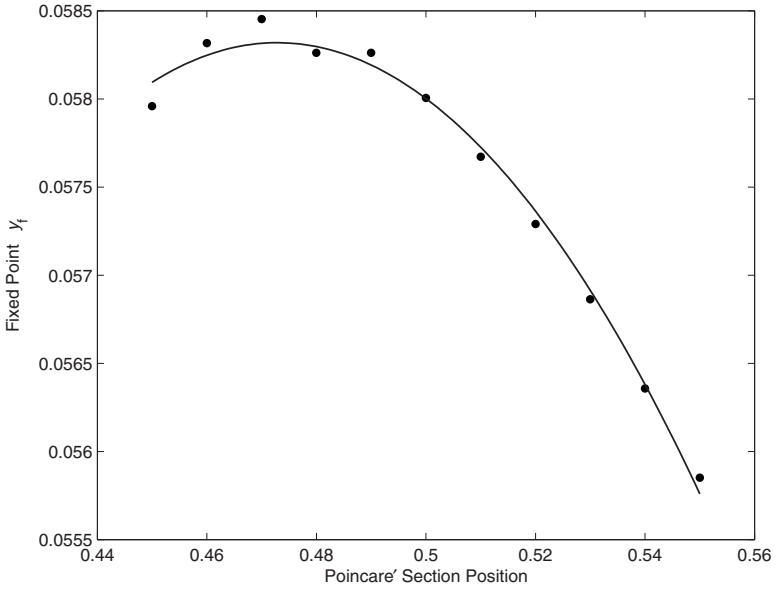

FIG. 5. Dependence of the fixed point y_f in the three-dimensional Poincaré region (dots). A quadratic (solid line) has been fitted to the data using least-squares regression.

the uncontrolled nominal reactor operation with $\theta=0.1095$. The comparative results are shown in Fig. 9. Again, it can be seen that the Q2D-SPF controller gives better controller performance than the L2D-SPF controller.

The L2D-SPF and Q2D-SPF controllers were then compared over a range controller sampling intervals, and the results are shown in Figs. 10 and 11. Simulations were performed at sampling intervals within the range $0.01\ \text{h} \leq T_s \leq 0.04\ \text{h}$, and the performance of the L2D-SPF and Q2D-SPF controllers was evaluated by comparing the values of Y at the thin Poincaré region. The results demonstrate that the Q2D-SPF controller performs better than the L2D-SPF controller for most choices of sampling interval.

Finally, a comparison of the relative effectiveness of the traditional SPF and the proposed L2D-SPF and Q2D-SPF is shown in Fig. 12 for simulations performed at sample time intervals ranging between $0.01\ \text{h} \leq T_s \leq 0.10\ \text{h}$. The vertical axis in the plot shows the MSE values of both controller types at the different sampling rates. The MSE is calculated as in Eq. (11). From Fig. 12, it may be seen that the MSEs for the 2D-SPF controllers are substantially less than the MSEs for the original SPF controller. Moreover, the conventional SPF controller fails when $T_s \geq 0.07\ \text{h}$ while the 2D-SPF controllers successfully stabilize the chaotic trajectory to its period-1 UPO. Hence, this demonstrates the effectiveness of the proposed 2D-SPF controllers in scenarios when only limited frequency measurements are accessible for closed-loop control.

V. CONCLUSIONS

Linear (L2D-SPF) and quadratic (Q2D-SPF) two-dimensional sampled data control algorithms have been proposed in this paper. These two-dimensional control algo-

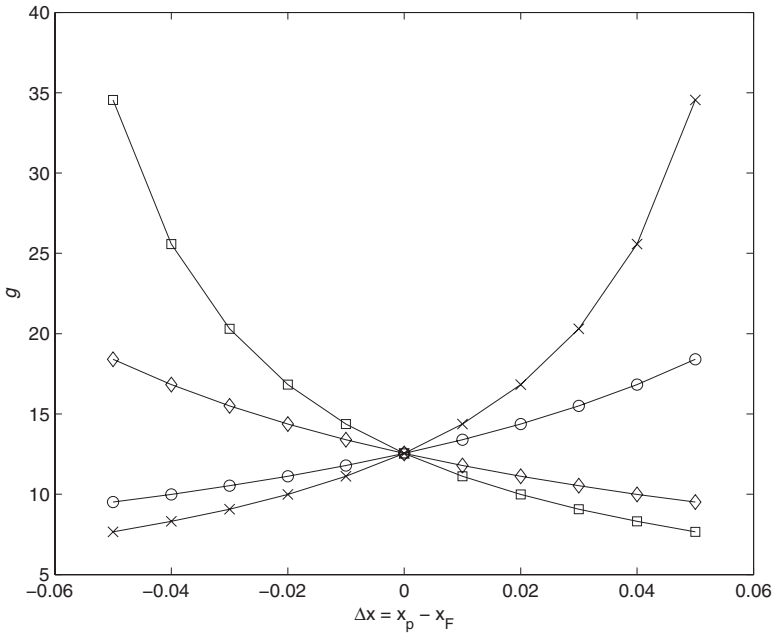

FIG. 6. Dependence of feedback gain g on Δy and Δx for the L2D-SPF controller. ◯: $\Delta y = 0.001$. ×: $\Delta y = 0.002$. □: $\Delta y = -0.001$. ◇: $\Delta y = -0.002$.

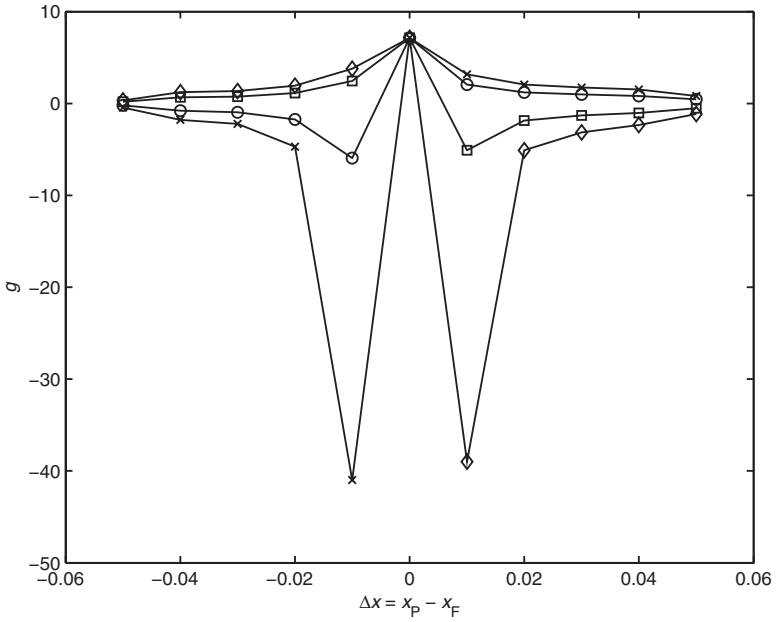

FIG. 7. Dependence of feedback gain g on Δy and Δx for the Q2D-SPF controller. ◯: $\Delta y = 0.001$. ×: $\Delta y = 0.002$. □: $\Delta y = -0.001$. ◇: $\Delta y = -0.002$.

rithms are based upon the original SPF controller, but they are designed using a series of Poincaré maps at different sampled points within a finite Poincaré region in the phase space. The fixed points of the series of Poincaré maps may be expressed as linear (L2D-SPF) or quadratic (Q2D-SPF) functions, respectively. The use of a series of Poincaré maps explicitly accounts for the dependence of the fixed point on the sampled point in the phase space, allowing the specification of control algorithms whose gain varies according to the distance of the sampled point from the nominal theoretical Poincaré section.

Using simulations of a mutating autocatalytic reaction in a CSTR, the performance of the conventional and our SPF controllers were compared across a range of sampling rates. It was shown that the proposed controllers provide superior control performance compared to the conventional SPF controller when the measurement sampling rate is decreased. In the study, the width of the Poincaré region in the phase space was fixed as $0.44 \leq X \leq 0.56$. However, it is expected that there will be an optimum width of the Poincaré region for a specific choice of the sampling rate. The optimum Poincaré region thickness is not investigated in this paper, and further work is required to investigate this relationship.

In the derivation of these controllers, the various Poincaré maps of the attractor are assumed to be stationary in presence of manipulated variable perturbations. It is assumed that changes in the position of the fixed point due to manipulated variable perturbations are along the attractor. The current manipulated variable of the 2D control law does not inherit a component of the previous manipulated variable perturba-

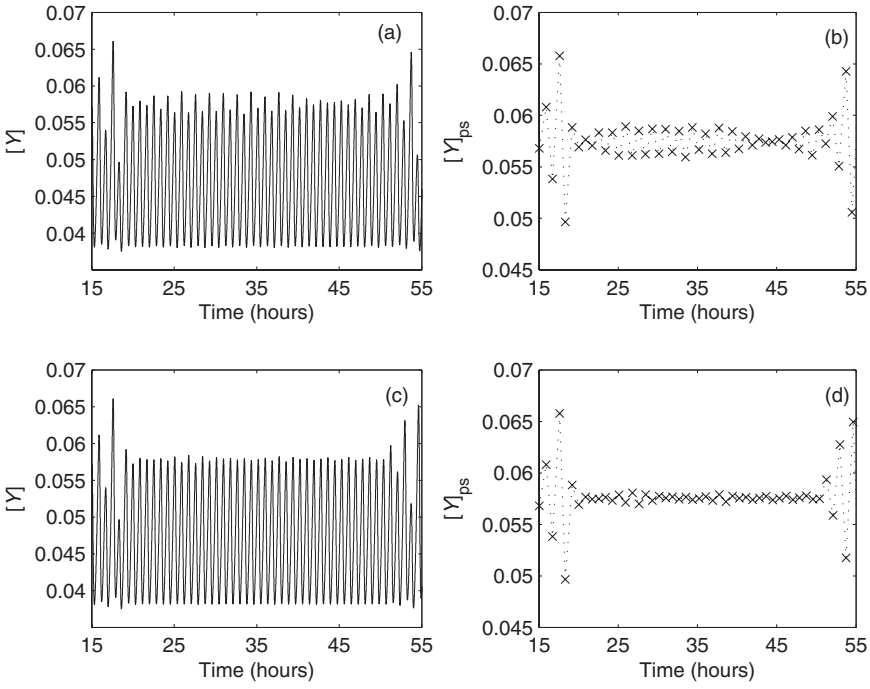

FIG. 8. Comparison of linear and quadratic discrete SPF controller performances at $T_s = 0.01$ h (no noise). Panel (a): y with L2D-SPF controller. Panel (b): y at the thin Poincaré region with L2D-SPF. Panel (c): y with Q2D-SPF controller. Panel (d): y at the thin Poincaré region with Q2D-SPF.

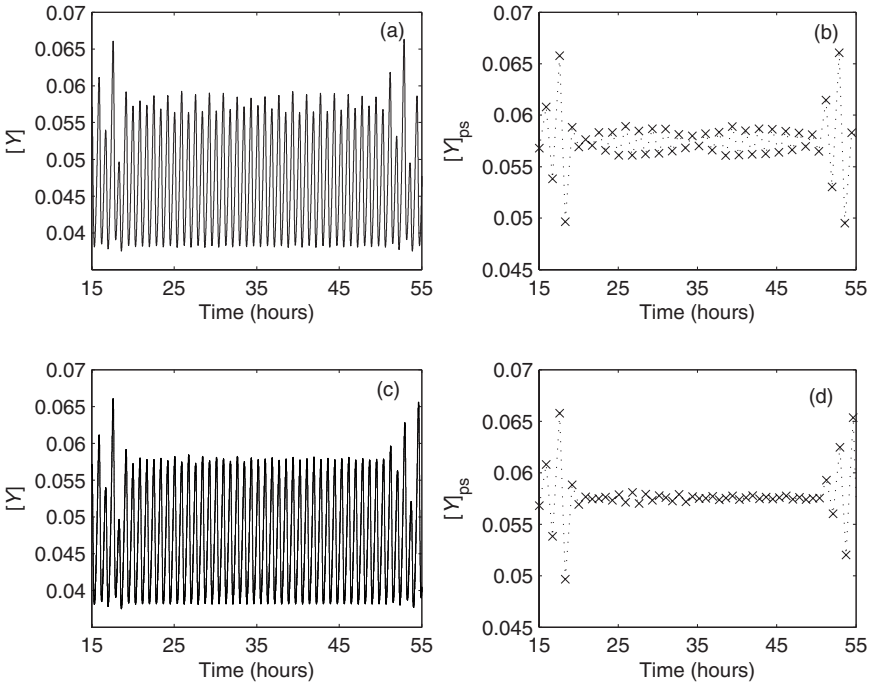

FIG. 9. Comparison of L2D-SPF and Q2D-SPF controller performances with noisy concentration measurements at $T_s=0.01$ h. Panel (a): y with L2D-SPF controller. Panel (b): y at the thin Poincaré region with L2D-SPF. Panel (c): y with Q2D-SPF controller. Panel (d): y at the thin Poincaré region with Q2D-SPF.

tion. However, the derived 2D control laws may be further extended by incorporating the effect of past manipulated variable perturbations. Such a modification may be necessary if the fixed point of the Poincaré map changes position away from the nominal attractor due to manipulated variable perturbations. Hence, to design a control algorithm, the variation of the fixed point of the Poincaré map due to inaccuracies in sampling and the effect of past parametric perturbations may need to be considered.

Modifications of the 2D algorithms presented here could also be further extended to the general case, where the Poincaré region is of higher dimension. High-dimensional chaos is common in real experimental systems [20] and in systems where the attractor is reconstructed from time delay measurements of a single observable state variable [21]. Higher-dimensional SPF algorithms incorporating the functional dependence of the fixed point on the Poincaré section position will be investigated in future studies.

Most experimental systems are subjected to effects of noise in the measured state variable. The dynamical noise in a system may change the bifurcation behavior of a nonlinear dynamical system and the noise in the measurements makes the detection of chaos difficult and generates noise induced transitions. Noise also forces the trajectory to leave its stable manifold even in the presence of closed loop control. The proposed 2D-SPF algorithms have been shown to perform

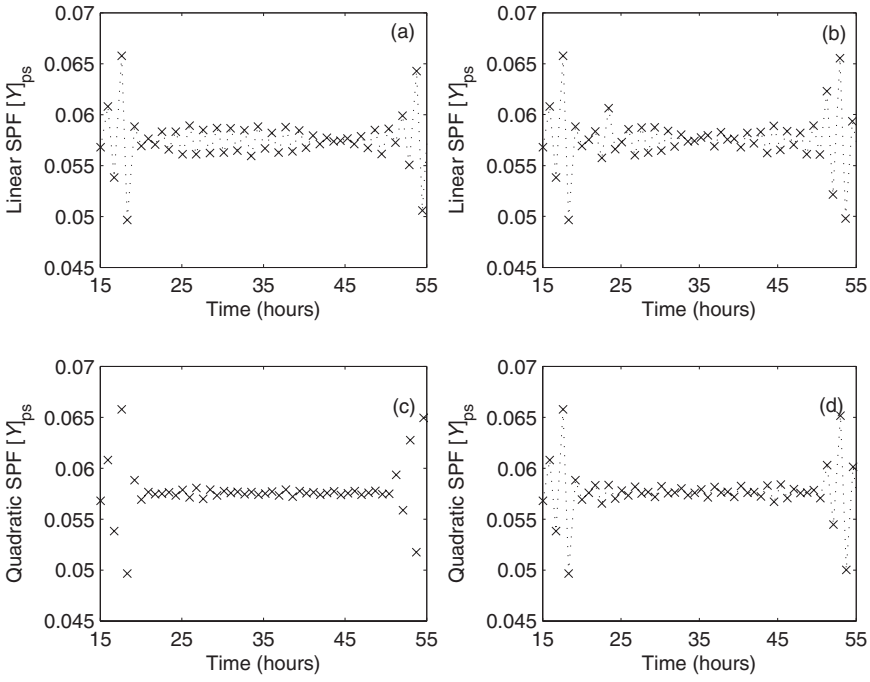

FIG. 10. Comparison of Y concentrations at thin Poincaré region for L2D-SPF and Q2D-SPF controllers for different sampling intervals. Panels (a) and (c): $T_s=0.01$ h. Panels (b) and (d): $T_s=0.02$ h.

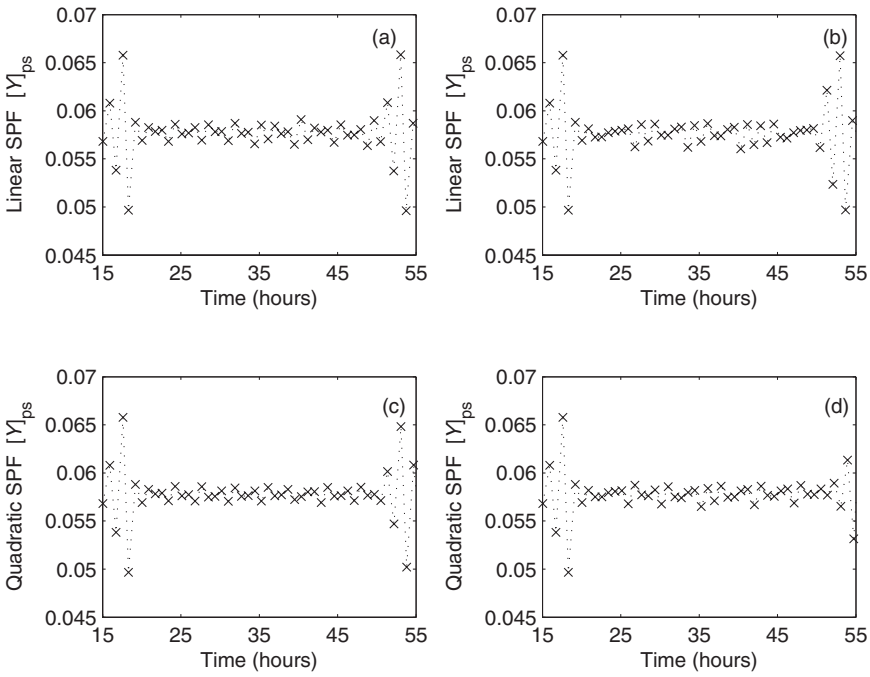

FIG. 11. Comparison of Y concentrations at thin Poincaré region for L2D-SPF and Q2D-SPF controllers for different sampling intervals T_s. Panels (a) and (c): $T_s = 0.03$ h. Panels (b) and (d): $T_s = 0.04$ h.

better than the single-dimensional counterpart when noisy process data is available for measurement and control.

Experimental systems may also be influenced by parametric drift in its variables. As the parameters drift away from their nominal values, the bifurcation behavior and the shape of the attractor may change. However, if predominant bifurcation characteristics are preserved, then the existence of a finite Poincaré region in phase space would ensure a sufficient number of intersections of the attractor. Hence, it is expected that the 2D-SPF algorithms would exhibit better performance in conditions when parametric drift is not negligible. However, further systematic study of an experimental system is required to quantify the effect of parametric drift on the 2D-SPF algorithms.

The implementation of the 2D-SPF control laws assumes that sufficient concentration data are available to generate the individual Poincaré maps spanning the Poincaré region. This prerequisite may limit the practicality of the proposed algorithms if concentration measurements from an actual reaction system are noise corrupted or are subject to sampling constraints. The sampling constraint may arise because in most practical situations the sampling frequency depends on the speed of the measurement device. In such instances, alternative methods may be required to generate the Poincaré maps. Alternatively, if species concentration data are not available at a sufficiently high frequency, then a new control strategy may be required. In such cases when sufficient species concentrations are not measurable, an inferential control strategy

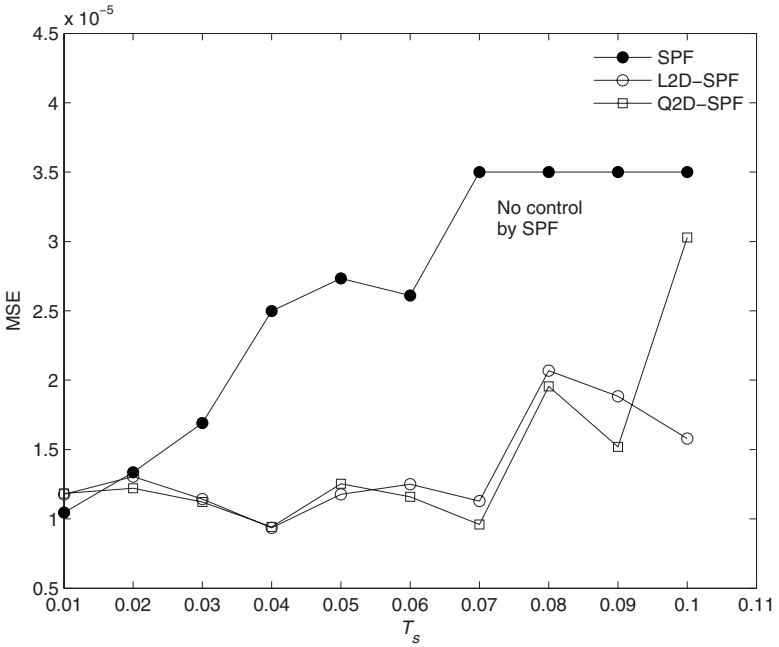

FIG. 12. Comparison of SPF controller performances in terms of the MSE of a period-1 fixed-point target with increasing sample time interval T_s.

may be of benefit. This would use a more easily measured (secondary) state variable to control the difficult to measure concentrations. The instantaneous rate of heat evolution or *p*H measurements offer potential measured secondary variables for chemical systems.

VI. NUMERICAL SIMULATION

All the simulations were performed in MATLAB7.1 using the variable order solver ode15s. The relative tolerance was selected as 10^{-12} and the absolute tolerance as 10^{-16} consistently for all simulations.

ACKNOWLEDGMENTS

The authors would like to thank the U.K. Engineering and Physical Sciences Research Council (Grant No. EPSRC GR/S85368/01) for funding this research.

[1] E. Ott, C. Grebogi, and J. A. Yorke, Phys. Rev. Lett. **64**, 1196 (1990).
[2] J. S. Lee and K. S. Chang, J. Process Control **6**, 71 (1996).
[3] B. Peng, V. Petrov, and K. Showalter, J. Phys. Chem. **95**, 4957 (1991).
[4] D. J. Gauthier, Am. J. Phys. **71**, 750 (2003).
[5] S. Boccaletti, C. Grebogi, Y. C. Lai, H. Mancini, and D. Maza, Phys. Rep. **329**, 103 (2000).
[6] T. Shinbrot, Adv. Phys. **44**, 73 (1995).
[7] P. Garhyan and S. S. E. H. Elnashaie, Ind. Eng. Chem. Res. **43**, 1260 (2004).
[8] P. Garhyan and S. S. E. H. Elnashaie, Chem. Eng. Sci. **59**, 3235 (2004).
[9] M. L. Davies, P. A. Halford-Maw, J. H. Hill, M. R. Tinsley, B. R. Johnson, S. K. Scott, I. Z. Kiss, and V. Gaspar, J. Phys. Chem. A **104**, 9944 (2000).
[10] P. Parmananda, P. Sherard, R. W. Rollins, and H. D. Dewald, Phys. Rev. E **47**, R3003 (1993).
[11] A. Garfinkel, M. L. Spano, W. L. Ditto, and J. N. Weiss, Science **257**, 1230 (1992).
[12] V. Petrov, B. Peng, and K. Showalter, J. Chem. Phys. **96**, 7506 (1992).
[13] R. W. Rollins, P. Parmananda, and P. Sherard, Phys. Rev. E **47**, R780 (1993).
[14] A. E. Abasaeed, Bioprocess Biosyst. Eng. **22**, 337 (2000).
[15] P. Gray and S. K. Scott, Ber. Bunsenges. Phys. Chem **90**, 985 (1986).
[16] J. H. Merkin, D. J. Needham, and S. K. Scott, Proc. R. Soc. London, Ser. A **406**, 299 (1986).
[17] P. Gray and S. K. Scott, *Chemical Oscillations and Instabilities* (Clarendon Press, Cambridge, England, 1990).
[18] M. L. Davies and S. K. Scott, Chem. Eng. Sci. **56**, 4587 (2001).
[19] A. E. Abasaeed (private communication).
[20] C. Grebogi and Y. C. Lai, IEEE Trans. Circuits Syst., I: Fundam. Theory Appl. **44**, 971 (1997).
[21] U. Dressler and G. Nitsche, Phys. Rev. Lett. **68**, 1 (1992).